energies

MDPI

Article

Detection of Internal Short Circuit in Lithium Ion Battery Using Model-Based Switching Model Method

Minhwan Seo [1], Taedong Goh [2], Minjun Park [1], Gyogwon Koo [1] and Sang Woo Kim [1,*]

[1] Department of Electrical Engineering, Pohang University of Science and Technology, 77 Cheongam-Ro, Nam-Gu, Pohang 37673, Korea; mhseo09@postech.edu (M.S.); parkmj@postech.edu (M.P.); ggkoo99@postech.edu (G.K.)

[2] Department of Creative IT Excellence Engineering and Future IT Innovation Laboratory, Pohang University of Science and Technology, 77 Cheongam-Ro, Nam-Gu, Pohang 37673, Korea; ehd1116@postech.edu

* Correspondence: swkim@postech.edu; Tel.: +82-54-279-2237; Fax: +82-54-279-2903

Academic Editor: Kwok Tong Chau
Received: 22 November 2016; Accepted: 3 January 2017; Published: 10 January 2017

Abstract: Early detection of an internal short circuit (ISCr) in a Li-ion battery can prevent it from undergoing thermal runaway, and thereby ensure battery safety. In this paper, a model-based switching model method (SMM) is proposed to detect the ISCr in the Li-ion battery. The SMM updates the model of the Li-ion battery with ISCr to improve the accuracy of ISCr resistance R_{ISCf} estimates. The open circuit voltage (OCV) and the state of charge (SOC) are estimated by applying the equivalent circuit model, and by using the recursive least squares algorithm and the relation between OCV and SOC. As a fault index, the R_{ISCf} is estimated from the estimated OCVs and SOCs to detect the ISCr, and used to update the model; this process yields accurate estimates of OCV and R_{ISCf}. Then the next R_{ISCf} is estimated and used to update the model iteratively. Simulation data from a MATLAB/Simulink model and experimental data verify that this algorithm shows high accuracy of R_{ISCf} estimates to detect the ISCr, thereby helping the battery management system to fulfill early detection of the ISCr.

Keywords: internal short circuit resistance; model updating method; battery safety

1. Introduction

Li-ion batteries have high power density, high energy efficiency and a long cycle life [1], and are therefore used as electric energy storage and power sources for electric devices and electric-drive vehicles. However, the Li-ion battery can develop dangerous malfunctions [2,3] such as internal short circuit (ISCr) [4,5] and cell reversal [6]; the main causes of these phenomena are overcharge [7] and overdischarge [8]. The ISCr may cause thermal runaway when the temperature rise by the ISCr in the battery exceeds a certain point [5] or the ISCr resistance R_{ISCf} is lower than a certain value [9]. Then a fire and an explosion can occur by the thermal runaway [10–12]. The ISCr is the main cause of battery fire accidents in Boeing 787-8 aircraft [13]. Therefore, a method to detect the ISCr is necessary before the thermal runaway happens in the Li-ion battery.

For these reasons, studies to detect the ISCr have been presented [14–17]. The ISCr can be detected by determining certain thresholds such as reduction of terminal voltage and increase of batteries temperature [14], but to obtain the thresholds, this method requires prior ISCr tests with batteries. Therefore, model-based algorithms have been presented to detect the ISCr by identifying variations of parameters in the model [15,16]. Using equivalent circuit models of a normal battery and a battery with ISCr as thresholds, characteristic parameters are obtained to detect ISCr in a battery pack [15], but this method can be used only when the battery with ISCr is connected to several normal batteries

in series, and the terminal voltages of both the battery with ISCr and the normal batteries are provided. The ISCr can be detected by using variation of estimated parameters in the equivalent circuit model and the energy balance equation [16], but this method must be verified with other load current profiles to check whether the estimated parameters show similar variation. When the ISCr occurs in the Li-ion battery, the terminal voltage increases once the battery is recharged, but the voltage reaches a stable value [18]; R_{ISCf} can be calculated using the charging current and the terminal voltage. However, calculation of R_{ISCf} by this method requires knowledge of the specific charging current that makes the terminal voltage reach the stable value in the battery with ISCr.

An early version [17] of the algorithm proposed in this paper estimated R_{ISCf} by using self-discharge from the ISCr to detect it, but the accuracy of R_{ISCf} estimates was low; to solve this problem, this paper presents a model-based switching model method (SMM). As a fault index, R_{ISCf} is estimated accurately by using SMM to detect the ISCr. To verify the proposed algorithm, environments of simulation and experiment are configured and two load current profiles: dynamic stress test (DST) and urban dynamometer driving schedule (UDDS) are used. The proposed algorithm is explained in Section 2, the environments of simulation and experiment are introduced in Section 3. The results of the simulation and the experiment are presented and discussed in Section 4. Finally, the conclusion and outline of future work are presented in Section 5.

2. Switching Model Method

In accordance with the estimated state of charge (SOC) defined as the present capacity of the battery as a proportion of its total capacity, the model of Li-ion battery with ISCr is switched to the updated model of Li-ion battery with ISCr. If the variation between initial estimated SOC and current estimated SOC is $\geq$0.2, the R_{ISCf} is estimated. Estimates of R_{ISCf} fluctuate due to variation in load currents, so as a fault index, the mean $\overline{R_{ISCf}}$ of estimated R_{ISCf}s is used to detect the ISCr instead of the estimated R_{ISCf}. $\overline{R_{ISCf}}$ is calculated from the previous estimated R_{ISCf}s and the current estimated R_{ISCf}, then used to change the model with ISCr to the updated model with ISCr. Then, using the updated model improves the accuracy of open circuit voltage (OCV) estimates, so R_{ISCf} is estimated accurately. Iteratively, the next $\overline{R_{ISCf}}$ is calculated using the next estimated R_{ISCf} and used to update the model again. We call this process the SMM (Figure 1).

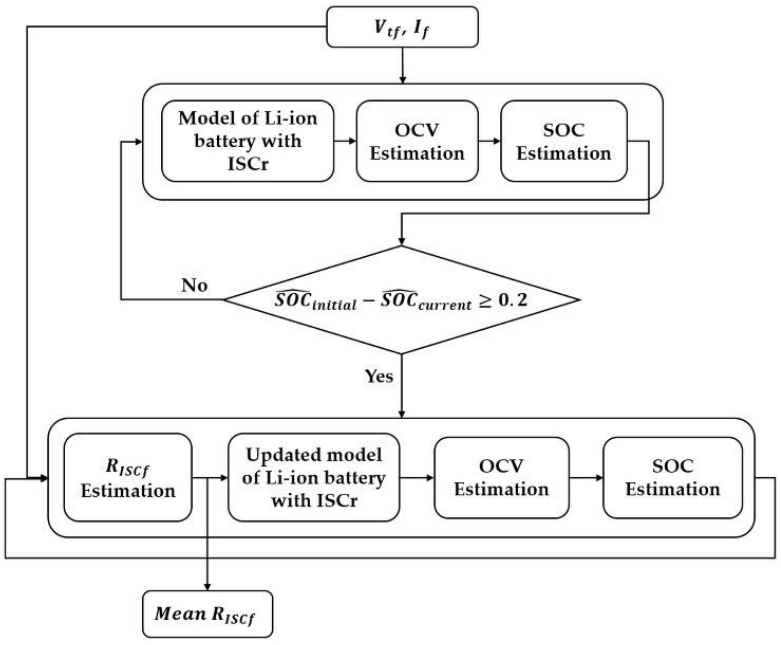

Figure 1. The scheme of the switching model method.

2.1. Equivalent Circuit Models

A normal Li-ion battery can be represented by an equivalent circuit model (Figure 2a) [15,17,19] that consists of OCV V_{oc}, internal resistance R, load current I and terminal voltage V_t. The Li-ion battery with ISCr can be represented by a similar equivalent circuit model (Figure 2b) [15,17,20] where I_{1f} is the current that flows within the battery, and I_{2f} is the current that flows through the R_{ISCf}.

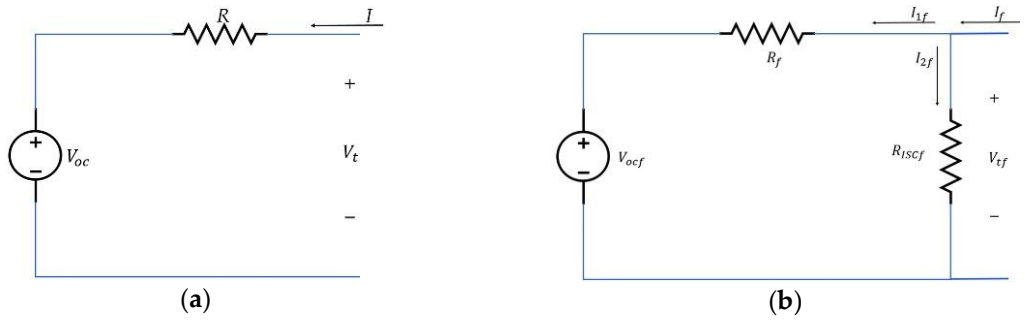

Figure 2. Schematic diagram of equivalent circuit models: (**a**) normal battery; (**b**) battery with ISCr.

This model with ISCr has been verified to mimic the ISCr [17]. Especially, subscript f (fault) is used to distinguish between parameters related to the model with ISCr and parameters of the normal battery model. The model with ISCr is described in Equations (1) and (2) by Ohm's law with a discretization step [15]:

$$I_f(k) = I_{1f}(k) + I_{2f}(k) \tag{1}$$

$$\begin{aligned} V_{tf}(k) &= V_{OCf}(k) + R_f I_{1f}(k) \\ V_{tf}(k) &= \frac{R_{ISCf}}{R_f + R_{ISCf}} V_{OCf}(k) + \frac{R_f R_{ISCf}}{R_f + R_{ISCf}} I_f(k) \end{aligned} \tag{2}$$

2.2. OCV Estimation

The recursive least squares (RLS) algorithm is usually used to estimate parameters in the normal battery model [19]. In this paper, the RLS algorithm was used to estimate model parameters such as V_{ocf} and R_f (Figure 2b). The initial value of the covariance matrix was [500 −250; −250 210], and initial values of the parameter vector θ_f that contains estimated parameters were the terminal voltage measured at the first time and 0.05. The forgetting factor is typically a value between 0.95 and 1 to get finely estimated parameters. In this study, the forgetting factor was set to 0.9995. To distinguish the OCV estimates from the two models with ISCr, $V_{OCf,pre}$ is the estimated OCV from the model with ISCr, and $V_{OCf,upd}$ is the estimated OCV from the updated model with ISCr. The equation used in the RLS algorithm is

$$\begin{aligned} y_f &= V_{tf}(k) = \theta_f^T \varnothing_f \\ \varnothing_f &= \left[1, I_f(k)\right] \\ \theta_f &= \left[\frac{R_{ISCf}}{R_f + R_{ISCf}} V_{OCf,pre}(k),\ \frac{R_f R_{ISCf}}{R_f + R_{ISCf}}\right] \end{aligned} \tag{3}$$

where y_f is a measurable quantity and $\varnothing_f$ is a vector of known quantities. The RLS algorithm cannot estimate R_{ISCf} directly, because the number of unknown parameters is bigger than the number of known parameters. In Equation (3), θ_f has two estimated parameters, $\frac{R_{ISCf}}{R_f + R_{ISCf}} V_{OCf,pre}$ and $\frac{R_f R_{ISCf}}{R_f + R_{ISCf}}$, which are combined with three unknown parameters, $V_{OCf,pre}$, R_f and R_{ISCf}.

Therefore, using the assumption [18] that the first parameter $\frac{R_{ISCf}}{R_f + R_{ISCf}} V_{OCf,pre}$ of θ_f can approximate $V_{OCf,pre}$ because the $R_{ISCf} >> R_f$, the $V_{OCf,pre}$ can be estimated from the RLS algorithm.

However, this approximation-assumption causes error that reduces the accuracy of R_{ISCf} estimates. Therefore, the updated model described in Equations (4) and (5) must be used to avoid this assumption.

$$\begin{aligned} I_{2f}(k) &= \frac{V_{tf}(k)}{R_{ISCf}} \\ I_{1f}(k) &= I_f(k) - I_{2f}(k) \end{aligned} \tag{4}$$

$$\begin{aligned} y_f = V_{tf}(k) &= \theta_f^T \varnothing_f \\ \varnothing_f &= \left[1, I_{1f}(k)\right] \\ \theta_f &= \left[V_{OCf,upd}(k), R_f(k)\right] \end{aligned} \tag{5}$$

If the initial R_{ISCf} is estimated at the point, at which the model with ISCr is switched to the updated model with ISCr, the unknown parameter R_{ISCf} is assumed to be the initial estimated R_{ISCf}. The $V_{OCf,pre}$ is used to estimate the initial R_{ISCf}, and the method to estimate SOC and R_{ISCf} will be explained in Section 2.3. Then the current I_{1f} can be calculated using Equation (4) and used as input data of the RLS algorithm in Equation (5). Once the input data changes from I_f to I_{1f}, the estimated parameters of θ_f also change and the $V_{OCf,upd}$ can be estimated directly without the approximation-assumption. Once the next R_{ISCf} is estimated using $V_{OCf,upd}$, $\overline{R_{ISCf}}$ is calculated and then used to update the model and estimate $V_{OCf,upd}$ iteratively.

After switching the model, the estimated OCVs with SMM began to be more accurate than the estimated OCVs without SMM (Figure 3) because of elimination of the error from the approximation-assumption. The true OCVs used for verification were calculated using the true value of R_{ISCf}, the coulomb counting method and the relation between OCV and SOC.

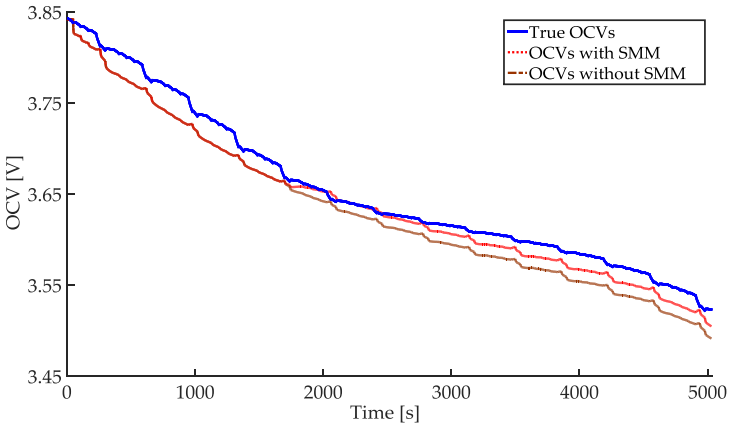

Figure 3. Comparison of true OCVs, estimated OCVs with SMM and estimated OCVs without SMM (experiment: cell A, DST 5 A and ISCr 20 Ω).

2.3. SOC and R_{ISCf} Estimation

The estimated SOCs can be obtained from the relation between OCV and SOC (Figure 4). Because of additional self-discharge due to I_{2f} flowing through the R_{ISCf}, the estimated SOCs decline more in the battery with ISCr than in the normal battery. Furthermore, decrease in R_{ISCf} represents increase in the severity of the ISCr in the Li-ion battery and in the decline of estimated SOCs. Using the self-discharge phenomenon, R_{ISCf} can be estimated [18].

The coulomb counting method is usually used to calculate true SOCs from the load current, true initial SOC and total capacity [21]. This method uses Equation (6) with a discretization step, where C_{max} is the maximum capacity of the battery, and T is the sampling rate. To eliminate the

unknown term $SOC_f(0)$, $SOC_f(k)$ is subtracted from $SOC_f(k+1)$, and I_{2f} is replaced with $I_{2f} = \frac{V_{tf}}{R_{ISCf}}$ in Equation (6).

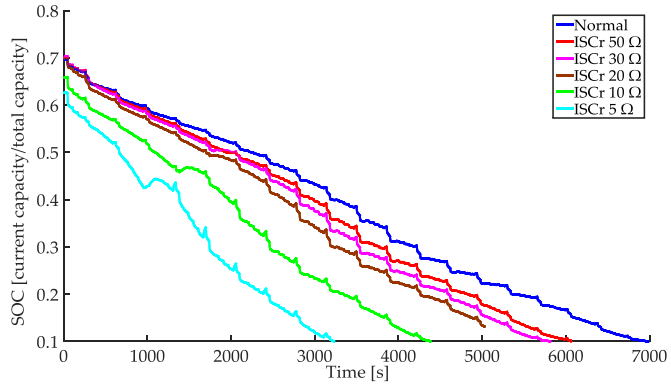

Figure 4. Comparison of estimated SOCs of normal cell and cell with ISCr (experiment: cell A, DST 5 A, ISCr 50 Ω, 30 Ω, 20 Ω, 10 Ω and 5 Ω).

Exact estimation of the R_{ISCf} by using the variation of estimated SOCs is difficult in the short interval between $k+1$ and k. Therefore, the interval must be increased by adding the $k-1$th to $p+1$th equations to the kth equation in Equation (7) to clearly show the self-discharge phenomenon where k is a current iteration and p is an initial iteration ($p+2 < k$).

$$SOC_f(k) = SOC_f(0) + \frac{T}{C_{max}} \sum_{n=1}^{k} \left[I_f(n) - I_{2f}(n) \right] \tag{6}$$

$$SOC_f(k+1) - SOC_f(k) = \frac{T}{C_{max}} I_f(k+1) - \frac{T}{C_{max}} \frac{V_{tf}(k+1)}{R_{ISCf}} \tag{7}$$

The first term on the right side of Equation (8) describes the discharge from the load current, and the second term represents the self-discharge from the ISCr. R_{ISCf} can be estimated using Equation (9), which is a rearrangement of Equation (8).

$$SOC_f(k) - SOC_f(p) = \frac{T}{C_{max}} \sum_{n=p+1}^{k} I_f(n) - \frac{T}{C_{max}} \frac{1}{R_{ISCf}} \sum_{n=p+1}^{k} V_{tf}(n) \tag{8}$$

$$R_{ISCf} = \frac{\frac{T}{C_{max}} \sum_{n=p+1}^{k} V_{tf}(n)}{\frac{T}{C_{max}} \sum_{n=p+1}^{k} I_f(n) + (SOC_f(p) - SOC_f(k))} \tag{9}$$

The choice of time to estimate the R_{ISCf} for switching the model is important, because if ISCr is 50 Ω, 30 Ω or 20 Ω, the self-discharge from the ISCr is not observed dominantly in the early iterations of the process of estimating SOC (Figure 4); i.e., the ratio of decrease in SOC due to self-discharge to total decrease in SOC must be large enough to reduce the effect of errors of the estimated SOCs and to clearly show the effect of self-discharge from ISCr. Accordingly, we determine that the model should be switched when the variation between initial estimated SOC and current estimated SOC is $\geq$0.2; i.e., 20% of the total capacity of the Li-ion battery.

3. Simulation and Experiment

3.1. Load Current Profiles

Two load current profiles were used as input data to the simulation and the experiments (Figure 5). We named these current profiles DST 5 A and UDDS 5 A; both have the minimum value of −5 A. We also used both DST 3 A and UDDS 3 A to verify the proposed algorithm with various data.

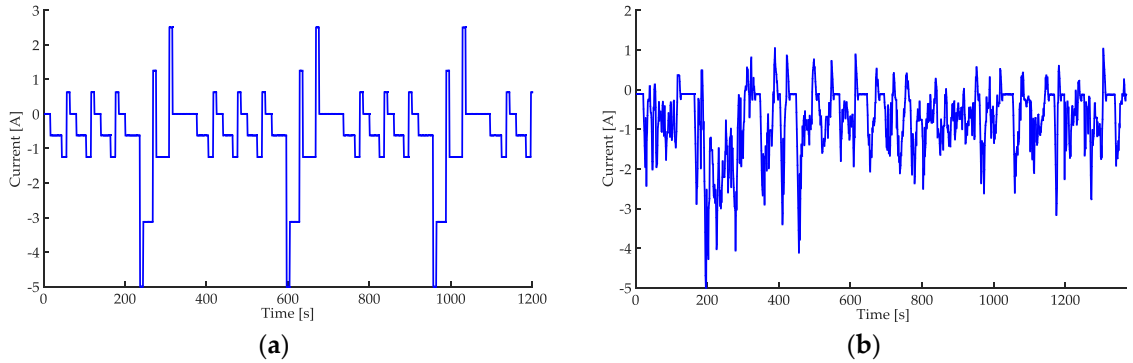

Figure 5. Load current profiles: (**a**) DST current profile; (**b**) UDDS current profile.

3.2. Configuration of Simulation Environment

In this study, a first-order RC model [22] was used to build a simulation model. To represent the ISCr, R_{ISCf} was connected in parallel at the terminal of the first-order RC model (Figure 6). The simulation model was configured using MATLAB/Simulink [23,24]. Resistance R_{0f}, resistance R_{1f} and capacitance C_{1f} (Figure 6) were estimated using the RLS algorithm with experimental data of cell A and DST 5 A [19], then used to build the simulation model.

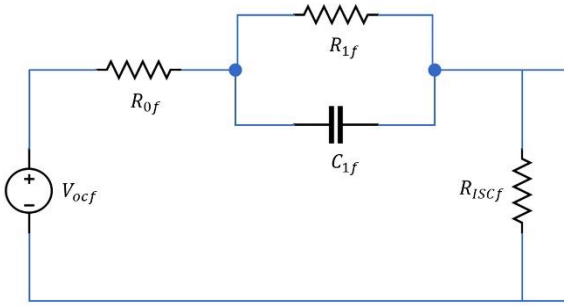

Figure 6. Configuration of simulation model: the first-order RC model with R_{ISCf}.

3.3. Configuration of Experiment Environment

In this study, two identical cells A and B (Table 1) were used to configure the experiment and to get data in various environments. The temperature was about 18–26 °C when cells A and B were tested. The initial SOC was set to 70% in both cells. The load current profiles were differently applied to each battery. DST 5 A and UDDS 5 A were used in experiments with cell A, and DST 3 A and UDDS 3 A were used for cell B. To prevent batteries from overdischarge, these load current profiles were applied to the batteries until their SOCs reached 10% of total capacity.

Table 1. Key specification of Li-ion battery.

Model	Type	Nominal Voltage	Nominal Capacity	Upper/Lower Cut-Off Voltage
INR 18650-20R	$LiNiCoMnO_2$	3.6 V	2000 mAh	4.2 V/2.0 V

To make various values of resistance such as 50 Ω, 30 Ω, 20 Ω, 10 Ω and 5 Ω, the five 10 Ω resistances were combined. The tolerance of the 10 Ω resistance was ±5%. The true values of these resistances were measured such as 49.91 Ω, 29.93 Ω, 19.92 Ω, 9.95 Ω and 4.98 Ω respectively, and used to calculate the relative error in the experimental data. When the load current profile was applied to the cell, the switch was used to connect the cell and resistances 50 Ω, 30 Ω, 20 Ω, 10 Ω or 5 Ω in

parallel to represent a battery with ISCr. In 10 s after the load current was sent, the switch was turned on. Therefore, the load current and the terminal voltage were measured after 10 s; sample interval was 0.1 s.

3.4. Relation between OCV and SOC Test

The relation between OCV and SOC was obtained by a prior test [25] and is necessary to use the proposed algorithm. After the battery had been charged fully, it was rested for 3600 s to obtain a value of OCV that is equal to the terminal voltage. Then the battery was discharged with 0.5 C for 720 s to set the SOC to 90%, then rested for 3600 s to get the value of OCV. The OCV-SOC curve (Figure 7) could be obtained by repeating the process until the value of SOC reached 0%.

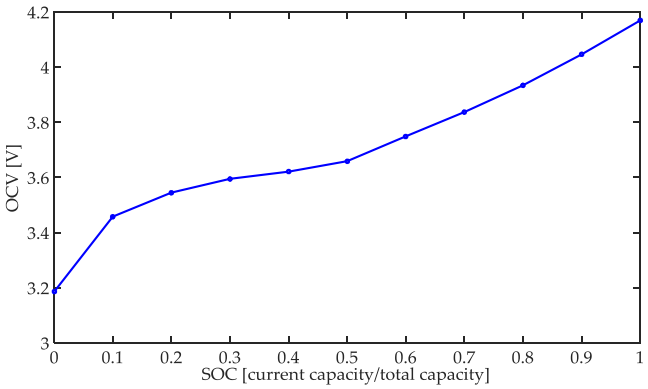

Figure 7. Relation between OCV and SOC.

4. Results

4.1. Comparison between Results with SMM and without SMM

To ensure fair comparison between $\overline{R_{ISCf}}$ estimates with and without SMM from the same point, the R_{ISCf}s were not estimated in the method without SMM before the model with ISCr was switched to the updated model with ISCr in the method with SMM. After switching the model, $\overline{R_{ISCf}}$ with SMM began to converge more accurately on the true value of 10 Ω than $\overline{R_{ISCf}}$ without SMM did (Figure 8). The reason of this superiority is that the estimated OCVs and SOCs became accurate due to the updated model, which removed the error imposed by the approximation-assumption. It is also reason that the R_{ISCf} was estimated with the accurate SOC estimates. When the proposed algorithm without the assumption was used, the accuracy of R_{ISCf} estimates was generally improved and the relative error of the final value of $\overline{R_{ISCf}}$ decreased greatly (Tables 2 and 3). Because the decrease in the magnitude of true R_{ISCf} represented increase in the error from the assumption, the difference between relative errors with and without SMM increased as the magnitude of true R_{ISCf} decreased.

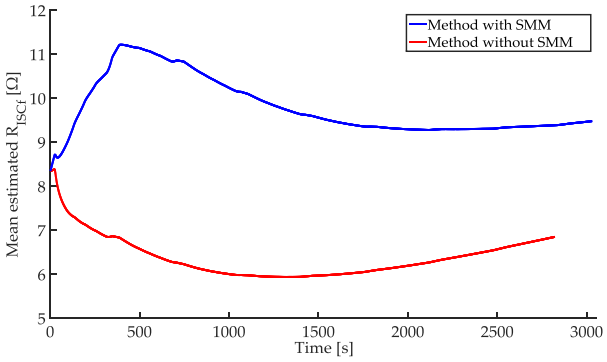

Figure 8. Comparison of $\overline{R_{ISCf}}$ with and without SMM (experiment: cell A, DST 5 A and ISCr 10 Ω).

Table 2. Relative error (%) of the final value of $\overline{R_{ISCf}}$ depending on the ISCr faults in the experiment with cell A and DST 5 A.

Method	True ISCr Resistance				
	5 Ω	**10 Ω**	**20 Ω**	**30 Ω**	**50 Ω**
With SMM	6.2	4.8	19.7	30.4	45.1
Without SMM	28.0	31.2	38.5	47.1	57.3

Table 3. Relative error (%) of the final value of $\overline{R_{ISCf}}$ depending on the ISCr faults in the experiment with cell A and UDDS 5 A.

Method	True ISCr Resistance				
	5 Ω	**10 Ω**	**20 Ω**	**30 Ω**	**50 Ω**
With SMM	12.3	16.0	18.9	34.3	49.3
Without SMM	48.8	44.4	38.0	49.5	61.8

4.2. Effect of Magnitude of True R_{ISCf} in the Simulation

Load current profiles DST 5 A and UDDS 5 A were used to execute the simulation model that represented cell A with ISCr. Initial SOC of the simulation model was 70%, like the configuration of the experiment with cells A and B.

In cases ISCr 50 Ω and 30 Ω for DST 5 A and ISCr 50 Ω, 30 Ω and 20 Ω for UDDS 5 A, the $\overline{R_{ISCf}}$s fluctuated much more than other ISCr faults (Figure 9) because the effect of self-discharge from ISCr was too small to be represented in the estimated outcomes like the normal battery.

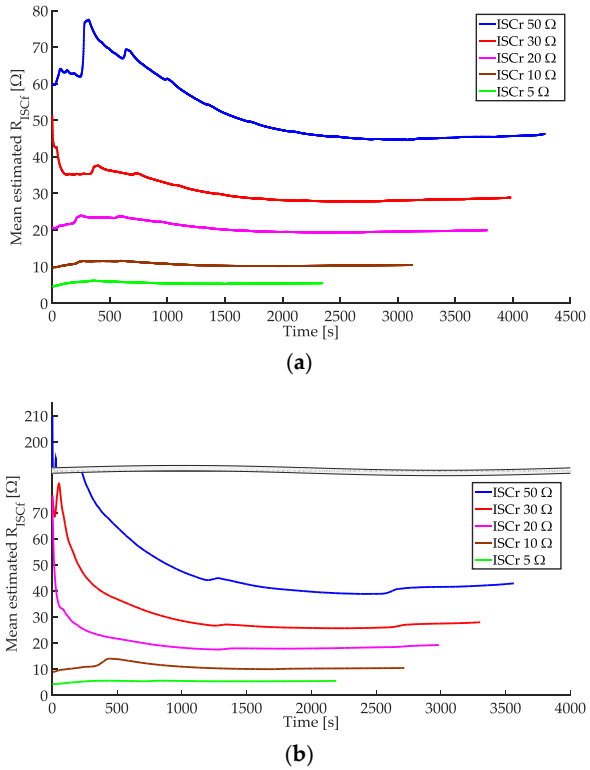

Figure 9. $\overline{R_{ISCf}}$ in the simulation model with ISCr 50, 30, 20, 10 and 5 Ω: (**a**) DST 5 A; (**b**) UDDS 5 A.

Although the fluctuations were high in the early stage, the magnitude of the fluctuations gradually decreased and $\overline{R_{ISCf}}$s converged on values near the true R_{ISCf}. The relative error of ISCr 5 Ω and

10 Ω was large although the self-discharge from ISCr 5 Ω and 10 Ω was influential. Because the self-discharge from ISCr 5 Ω and 10 Ω largely increased the decline of SOC in the early stage of interations (Figure 4), the initial estimated SOC had estimation error. This error affected the accuracy of R_{ISCf} estimates for ISCr 5 Ω and 10 Ω. The final value of $\overline{R_{ISCf}}$ had relative error ≤14.2% (Table 4) and the ISCr could be detected early with high accuracy of R_{ISCf} estimates.

Table 4. Relative error (%) of the final value of $\overline{R_{ISCf}}$ depending on the ISCr faults in the simulation model.

Discharge Condition	True ISCr Resistance				
	5 Ω	**10 Ω**	**20 Ω**	**30 Ω**	**50 Ω**
DST 5 A	9.7	4.6	0.2	3.7	7.5
UDDS 5 A	10.4	4.5	3.7	6.8	14.2

4.3. Effect of Magnitude of True R_{ISCf} in the Experiment with Cell A

$\overline{R_{ISCf}}$ also fluctuated in experimental results but also decreased and converged on values near the true R_{ISCf} (Figure 10). The main difference between simulation results and experiment results was that the maximum relative error of ISCr 50 Ω and 30 Ω significantly increased from 14.2% in the simulation to 49.3% in cell A (Table 5).

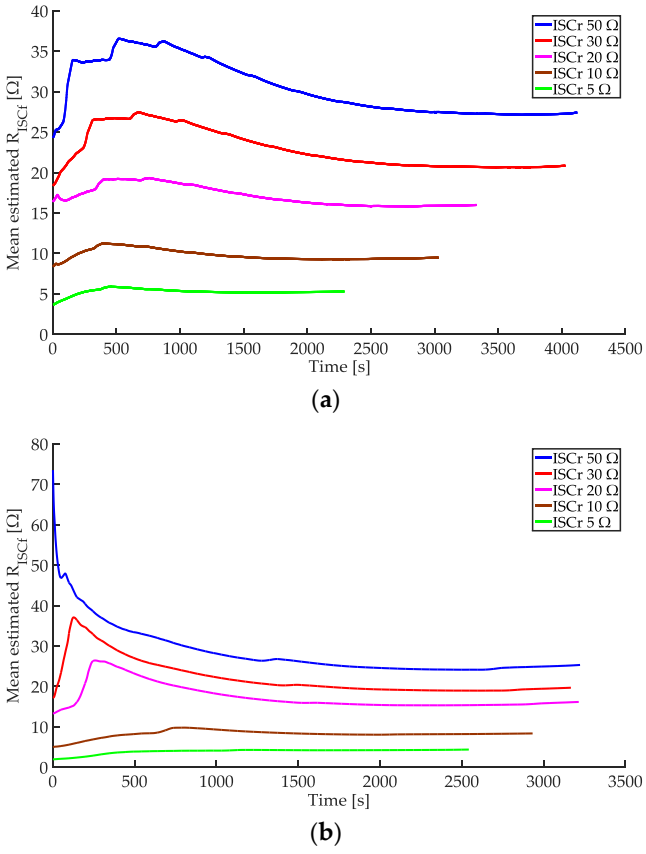

Figure 10. $\overline{R_{ISCf}}$ in the experiment with cell A with ISCr 50, 30, 20, 10 and 5 Ω: (**a**) DST 5 A; (**b**) UDDS 5 A.

Especially, when true R_{ISCf} was 50 Ω or 30 Ω, the effect of self-discharge from ISCr relatively decreased because the error of estimated SOCs increased due to noise in the experimental environment. Despite this noise, the ISCr 20 Ω, 10 Ω, and 5 Ω had relative error ≤19.7% because the effect of self-discharge from ISCr was much bigger than the increase of the error in estimated SOCs. Therefore,

the ISCr fault could be detected early before thermal runaway occurred in the Li-ion battery with ISCr. However, the low accuracy of estimated R_{ISCf} in ISCr 50 Ω and 30 Ω remains a problem; to overcome it, the effect of self-discharge from ISCr must be increased by decreasing the C-rate of the load current profiles to increase the time over which the battery completely discharges.

Table 5. Relative error (%) of the final value of $\overline{R_{ISCf}}$ depending on the ISCr faults in the experiment with cell A.

Discharge Condition	True ISCr Resistance				
	5 Ω	**10 Ω**	**20 Ω**	**30 Ω**	**50 Ω**
DST 5 A	6.2	4.8	19.7	30.4	45.1
UDDS 5 A	12.3	16.0	18.9	34.3	49.3

4.4. Effect of C-Rate of Load Current in the Experiment with Cell B

The experiment with cell B was conducted using DST 3 A and UDDS 3 A, which were the load current profiles with low C-rate. When the C-rate of load current profiles decreased, the area between the estimated SOCs of normal cell B and the estimated SOCs of cell B with ISCr 50 Ω increased more than that of cell A (Figure 11). The area represents the decline of SOC due to self-discharge by ISCr. Therefore, this change increased the influence of self-discharge, and the accuracy of the estimated R_{ISCf} in ISCr 50 Ω and 30 Ω was improved (Figure 12). Accordingly, the maximum relative error of ISCr 50 Ω and 30 Ω decreased greatly from 49.3% in cell A to 22.1% in cell B (Table 6), and the relative error was $\leq$26.1%.

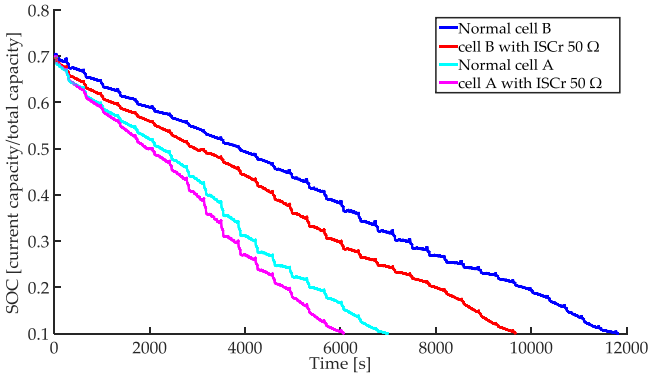

Figure 11. Comparison of estimated SOCs of normal cells and of cells with ISCr 50 Ω (experiments: DST 5 A for cell A and DST 3 A for cell B).

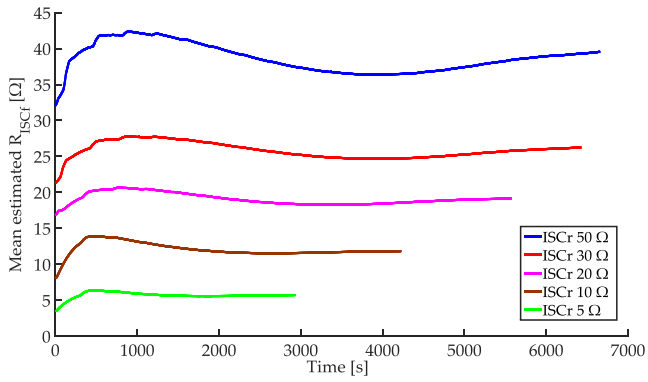

(**a**)

Figure 12. *Cont.*

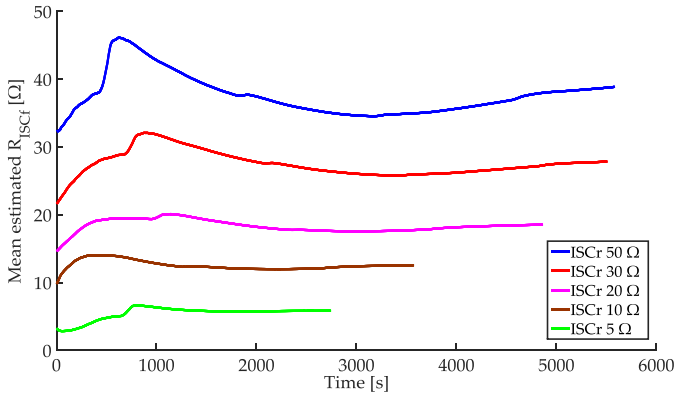

Figure 12. $\overline{R_{ISCf}}$ in the experiment with cell B with ISCr 50, 30, 20, 10 and 5 Ω: (**a**) DST 3 A; (**b**) UDDS 3 A.

Table 6. Relative error (%) of the final value of $\overline{R_{ISCf}}$ depending on the ISCr faults in the experiment with cell B.

Discharge Condition	True ISCr Resistance				
	5 Ω	**10 Ω**	**20 Ω**	**30 Ω**	**50 Ω**
DST 3 A	14.9	18.9	3.8	12.3	20.7
UDDS 3 A	17.3	26.1	6.9	6.9	22.1

4.5. Effect of Variation in OCV-SOC Curve

The OCV-SOC curve can be changed because of the capacity fade of Li-ion battery caused by the cycle aging and the calendar aging [3]. In this study, the amount of capacity fade of the aged battery (cell A) was 2.7% of total capacity. The OCV-SOC curves for both fresh cell A and aged cell A were almost equal. Therefore, the OCV-SOC curves for fresh cells A and B were used in the proposed algorithm. However, the severe capacity fade can cause significant change in the OCV-SOC curve. This change can generate the considerable error of estimated SOCs which results in the error of R_{ISCf} estimates in Equation (9).

In summary, when the load current pofiles with high C-rate were used, the ISCr fault in ISCr 20~5 Ω range could be detected early before thermal runaway happened in the Li-ion battery with ISCr. Furthermore, when the load current profiles with low C-rate were used to increase the effect of self-discharge in ISCr 50~30 Ω, the proposed algorithm could detect the ISCr fault early in ISCr 50~30 Ω with high accuracy of the R_{ISCf} estimates. In addition, the study considering the variation in the OCV-SOC curve should be proceeded continuously to improve the accuracy of the R_{ISCf} estimates.

5. Conclusions

In this paper, a model-based SMM is introduced to detect ISCr in the Li-ion battery. Using the equivalent circuit model of the battery with ISCr and the RLS algorithm, the OCV is estimated. The SOC is estimated by using its relationship with OCV. Then R_{ISCf} is estimated using the self-discharge phenomenon of the ISCr. The SMM greatly increased the accuracy of the estimated R_{ISCf}. The proposed algorithm was verified in simulations and experiments using two load current profiles. The effect of the magnitude of true R_{ISCf} on estimated R_{ISCf} and the effect of C-rate of load current on estimated R_{ISCf} were analyzed. The R_{ISCf} can be estimated with high accuracy using the proposed algorithm, and as fault index, the $\overline{R_{ISCf}}$ can be used to detect the ISCr early. Our future research will concentrate on extending our proposed algorithm to detection of ISCr in an aged battery and a battery pack.

Acknowledgments: This research was supported by the MSIP (Ministry of Science, ICT and Future Planning), Korea, under the "ICT Consilience Creative Program" (IITP-R0346-16-1007) supervised by the IITP (Institute for Information & communications Technology Promotion).

Author Contributions: Minhwan Seo suggested the main idea of this paper and constructed the proposed detection technique. Taedong Goh contributed the mathematical modeling and thoroughly reviewed the paper. Minjun Park conducted the experiments. Gyogwon Koo thoroughly reviewed the paper. Sang Woo Kim supervised the work and finally reviewed the paper.

Conflicts of Interest: The authors declare no conflict of interest.

References

1. Tarascon, J.M.; Michel, A. Issues and challenges facing rechargeable lithium batteries. *Nature* **2001**, *414*, 359–367. [CrossRef] [PubMed]
2. Balakrishnan, P.G.; Ramesh, R. Safety mechanisms in lithium-ion batteries. *J. Power Sources* **2006**, *155*, 401–414. [CrossRef]
3. Lu, L.; Han, X. A review on the key issues for lithium-ion battery management in electric vehicles. *J. Power Sources* **2013**, *226*, 272–288. [CrossRef]
4. Santhanagopalan, S.; Ramadass, P. Analysis of internal short-circuit in a lithium ion cell. *J. Power Sources* **2009**, *194*, 550–557. [CrossRef]
5. Zhao, R.; Liu, J. Simulation and experimental study on lithium ion battery short circuit. *Appl. Energy* **2016**, *173*, 29–39. [CrossRef]
6. Liu, Y.; Liu, Q. Failure study of commercial $LiFePO_4$ cells in over-discharge conditions using electrochemical impedance spectroscopy. *J. Electrochem. Soc.* **2014**, *161*, A620–A632. [CrossRef]
7. Leising, R.A.; Palazzo, M.J. A study of the overcharge reaction of lithium-ion batteries. *J. Power Sources* **2001**, *97*, 681–683. [CrossRef]
8. Maleki, H.; Howard, J.N. Effects of overdischarge on performance and thermal stability of a Li-ion cell. *J. Power Sources* **2006**, *160*, 1395–1402. [CrossRef]
9. Lithium-Ion Battery Safety: Detection of Developing Internal Shorts and Suppression of Thermal Runaway. Available online: http://www.camxpower.com/wp-content/uploads/4-6.pdf (accessed on 30 October 2016).
10. Feng, X.; Fang, M. Thermal runaway features of large format prismatic lithium ion battery using extended volume accelerating rate calorimetry. *J. Power Sources* **2014**, *255*, 294–301. [CrossRef]
11. Jhu, C.Y.; Wang, Y.W. Thermal runaway potential of $LiCoO_2$ and $Li(Ni_{1/3}Co_{1/3}Mn_{1/3})O_2$ batteries determined with adiabatic calorimetry methodology. *Appl. Energy* **2012**, *100*, 127–131. [CrossRef]
12. Zavalis, T.G.; Behm, M. Investigation of short-circuit scenarios in a lithium-ion battery cell. *J. Electrochem. Soc.* **2012**, *159*, A848–A859. [CrossRef]
13. Auxiliary Power Unit Battery Fire, Japan Airlines Boeing 787-8, JA829J, Boston, Massachusetts. January 7, 2013. Available online: http://www.ntsb.gov/investigations/AccidentReports/Reports/AIR1401.pdf (accessed on 21 October 2016).
14. Xia, B.; Mi, C.; Chen, Z. Multiple cell lithium-ion battery system electric fault online diagnostics. In Proceedings of the 2015 IEEE Transportation Electrification Conference and Expo (ITEC), Dearborn, MI, USA, 14–17 June 2015; pp. 1–7.
15. Ouyang, M.; Zhang, M. Internal short circuit detection for battery pack using equivalent parameter and consistency method. *J. Power Sources* **2015**, *294*, 272–283. [CrossRef]
16. Feng, X.; Weng, C. Online internal short circuit detection for a large format lithium ion battery. *Appl. Energy* **2016**, *161*, 168–180. [CrossRef]
17. Seo, M.; Goh, T.; Koo, G. Detection of internal short circuit in Li-ion battery by estimating its resistance. In Proceedings of the 4th IIAE International Conference on Intelligent System and Image Processing 2016 (ICISIP 2016), Kyoto, Japan, 8–12 September 2016; pp. 212–217.
18. Guo, R.; Lu, L. Mechanism of the entire overdischarge process and overdischarge-induced internal short circuit in lithium-ion batteries. *Sci. Rep.* **2016**, *6*, 1–9. [CrossRef] [PubMed]
19. He, H.; Zhang, X. Online model-based estimation of state-of-charge and open-circuit voltage of lithium-ion batteries in electric vehicles. *Energy* **2012**, *39*, 310–318. [CrossRef]
20. Kim, G.H.; Smith, K. Fail-safe design for large capacity lithium-ion battery systems. *J. Power Sources* **2012**, *210*, 243–253. [CrossRef]

21. Plett, G.L. Extended Kalman filtering for battery management systems of LiPB-based HEV battery packs: Part 2. Modeling and identification. *J. Power Sources* **2004**, *134*, 262–276. [CrossRef]
22. Liaw, B.Y.; Nagasubramanian, G. Modeling of lithium ion cells—A simple equivalent-circuit model approach. *Solid State Ion.* **2004**, *175*, 835–839.
23. Yao, L.W.; Aziz, J.A.; Kong, P.Y. Modeling of lithium-ion battery using MATLAB/simulink. In Proceedings of the IECON 2013—39th Annual Conference of the IEEE Industrial Electronics Society, Vienna, Austria, 10–13 November 2013; pp. 1729–1734.
24. Simulink Model of a Lithium-Ion Battery for the Hybrid Power System Test-Bed. Available online: http://www.learningace.com/doc/1488524/01a7c2704f7024d2b5c288c9e03efd0a/simulink-model-of-a-lithium-ion-battery-for-the-hybrid-power-system-testbed (accessed on 21 November 16).
25. Xing, Y.; He, W. State of charge estimation of lithium-ion batteries using the open-circuit voltage at various ambient temperatures. *Appl. Energy* **2014**, *113*, 106–115. [CrossRef]